IEEE Access
Multidisciplinary : Rapid Review : Open Access Journal

Received 25 February 2023, accepted 24 March 2023, date of publication 31 March 2023, date of current version 7 April 2023.

Digital Object Identifier 10.1109/ACCESS.2023.3263588

RESEARCH ARTICLE

Design and Fault Diagnosis of Induction Motor Using ML-Based Algorithms for EV Application

M. AISHWARYA AND R. M. BRISILLA
School of Electrical Engineering, Vellore Institute of Technology (VIT), Vellore 632014, India
Corresponding author: R. M. Brisilla (brisilla.rm@vit.ac.in)

ABSTRACT The need for alternate transportation is driven by the increased fossil fuel cost and the adverse effects of climatic change. Electric vehicles (EVs) are the best option as they have less carbon footprint and reduced dependency on fossil fuels. Prodigious efforts to enhance the efficiency of EVs resulted in the development of highly efficient three-phase induction motors. Difficulties in designing highly efficient induction motors (IM) with high torque and power factors hindered the success of EV applications. Hence, our aim is to diagnosis fault in the designed IM under variable load conditions. The proposed EV motor is designed for 415V, 50Hz, and 5HP output power rating using ANSYS RMxprt simulation software. A fault detection strategy is also implemented with various machine learning (ML) techniques like Support Vector Machine (SVM), K-nearest neighbors (k-NN), ML perceptron (MLP), Random Forest (RF), Decision Tree (DT), Gradient boosting (GB), Extreme Gradient Boosting (XGBoost), and Deep Learning (DL) for both healthy and faulty conditions. Short Circuit (SC), High Resistance connection (HRC), and Open-Phase circuit (OPC) are considered as faulty states for this study. Motor performance with variable load for all the states healthy and faulty are evaluated through machine learning.

INDEX TERMS Induction motor, electric vehicle, motor design, material, ANSYS, machine learning algorithms.

I. INTRODUCTION

Automobile sector is playing a vital part in the world's economic growth. Internal combustion vehicles used in most vehicles consume directly the fossil fuel and create a large amount of greenhouse gases affecting the entire world. This paved the way to discover new energy vehicles as an alternative to conventional vehicles, which are Electric Vehicles (EVs) [1], [2], [3]. The core part of an EV is the electric motor which converts electric energy to mechanical energy. Hence it is necessary to build an electric motor that enhances the efficiency of EV and its performance [4]. Induction Motor (IM), Brushless DC motor (BLDC), and Permanent Magnet Synchronous motor (PMSM) are the most commonly used motors for commercial purposes [5]. IM is more effective and economical than other motors due to its reliability, simple mechanical design, and effective field-weakening characteristics [6], [7]. However, the limitations such as core loss, friction loss, and copper loss, reduces the efficiency of IM [8], [9]. To overcome these limitations and to enhance the efficiency, researchers are focusing to optimize the length of the stator as it can also reduce harmonic losses. Also, IM characteristics are influenced by geometric dimensions like core length and size of the stator and rotor slots [10]. The motor's efficiency is also determined by the materials used for manufacturing [11], [12]. Several materials have been used for the motor design for many years, and the most often used materials for core & winding are Iron (Fe), Carbon steel 1008, and steel 1010 laminated cores, Aluminium (Al), Copper (Cu), and Silver (Ag). Traditionally, Al is used as winding material for IM but the Conductivity is lower than Cu [13].

Though Cu has high conductivity and increased mechanical efficiency than Al, it is costly. Ag, which has higher conductivity than Cu is expensive with a low melting point [14]. Hence, selecting winding materials and core lamination is vital for achieving higher efficiency and effective motor operation. In addition to material selection, the

The associate editor coordinating the review of this manuscript and approving it for publication was R. K. Saket.

fault detection (FD) system has also been used an effective approach to increase the performance of motor operation in EVs.

Researchers are developing FD strategies for IM based on two approaches. They are Model-based approaches and Data-driven approaches. Model-based approaches attempt to predict the faulty behavior by mathematically modelling the motor. The main disadvantage of this methodology is due to the machine's natural wear, because the degradation of machine components causes a difference between the actual machine and its mathematical model, when the fault magnifies. Furthermore, it is critical that the model assumes that the machine parameters are available, which does not always happen. This makes the diagnosis more challenging because it is necessary to estimate the machine parameters for the appropriate modelling of the machine [15], [16]. Data-driven approaches do not require IM model as well as the characteristics of the motor and load coupled to the machine. Furthermore, these methods have been widely used in fault diagnosis of nonlinear complex and time-varying systems and demonstrated promising outcomes in identifying faults. Machine learning (ML) is a most popular data driven approach which includes the k-Nearest Neighbor (k-NN) method, Naive Bayes (NB), Support Vector Machines (SVM), and Artificial Neural Networks (ANN) [15], [17], [18], [19], [20]. Deep Learning (DL) architectures have attracted the attention of several researchers, mainly those based on Convolutional Neural Networks (CNN). These algorithms are able to extract the failure characteristics of signals, as well as eliminate the need for a priority knowledge, allowing efficient independent fault diagnosis in electrical machines [21], [22], [23], [24], [25].

Data-driven FD techniques using ML and DL algorithms are being the recent focus by researches in diagnosing the motor faults. Many research findings are reported to detect the stator faults through monitoring the vibration and current signals extracted from the stator [26], [27], [28]. However, the detection of motor wiring or connection failures of IM has received the least attention. It is important to note that catastrophic failure modes, such as open-phase circuit (OPC), High Resistance Connections (HRC) in IM connections, are common. These failure modes are rare and their maintenance cost is also high. Furthermore, in most cases, these faults are caused due to human error during manufacturing. Various methods have been used to identify HRC. Thermal imaging is a valuable and effective approach for manual inspections. However, the process is expensive and complex [19]. Online detection techniques have been developed since past few decades, primarily based on resistance estimation or current sequence analysis. In a study [29], resistance is calculated by injecting voltage pulses with the inverter fixed in the drive. But, it requires the measurement of voltage between the motor's neutral and the DC-negative link terminal. The main disadvantage of this method is the requirement for an additional sensor and also the neutral point is accessed frequently.

In [30] and [31], induction motor model is designed with the consideration of HRC and short circuits (SC). These models are used to predict the negative sequence current and voltage resulting from unbalance to determine the type of failure (HRC or SC). In a similar technique is presented in [32], but the drive control strategy is employed to calculate the negative sequence current and voltage to design fault-tolerant control. Few studies discuss the detection of OPC fault, when it occurs at the motor connection. Park's Vector Approach is one of the most popular approach for this OPC fault. There are also model-based methods, such as the one described in [19], where a model is suggested and validated for open-circuit defects in the phases and wiring. As stated in [33], data driven fault detection and diagnosis (FDD) strategies based on ML or DL have become a feasible alternative fault detection technique for electric motors. Several reports has been published demonstrating the use of ML or DL to identify stator defects [34], [35], [36].

Hence, this paper presents data driven ML for FDD of IM and its design using Finite Element Analysis (FEA) techniques using ANSYS software. A data-driven approach is employed for SC fault, HRC fault, and OPC fault diagnosis in IM. A 4Pole, 415V, 5HP, 50Hz IM is designed using ANSYS. The data required for FDD is extracted from the motor designed, for the healthy and faulty conditions. The data extracted from various conditions (SC, HRC, and OPC) are given to the ML algorithms to identify the performance of IM. The different algorithms used to diagnosis the healthy and faulty status of the IM are Support Vector Machine (SVM), K-nearest neighbors (k-NN), ML perceptron (MLP), Random Forest (RF), Decision Tree (DT), Gradient boosting (GB), Extreme Gradient Boosting (XGBoost), and Deep Learning (DL). In [17] and [18], the authors used instantaneous output signals such as vibration and current signals of IM for FD, whereas this article considers RMS values of current, torque, slip, and efficiency. In addition, this manuscript considers multiple faults namely SC, HRC, and OPC which are not addressed in many of the articles. Also, FD of multiple faults requires multiclass labeling and hence RMS data is considered. Moreover, RMS data can reduce the computational complexity when compared to instantaneous data. This paper is divided into five sections: Section II explain the design of Induction motor. Section III gives Finite Element analysis of Motor. Section IV examines the different ML techniques using the data extracted from the motor. Section V presents the conclusion of the article and the potential future work.

II. DESIGN OF INDUCTION MOTOR

Designing the motor based on the application can provide efficient operation. Also, selection of motor size is one of the most challenging step in the design process. In this paper, IM is designed for the specifications given in Table. (1). RMxprt tool is used to design the rotor and stator geometry. The rotor and stator diameters, number of slots, iron core length, insulation material, and winding material are considered as the parameters to design the IM.

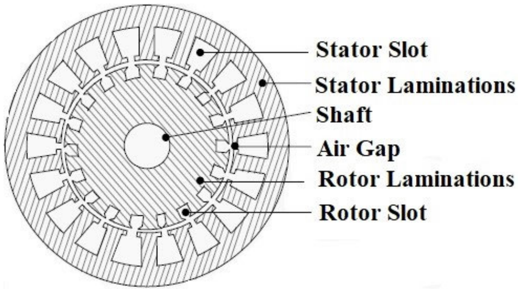

FIGURE 1. Cross sectional view of IM.

TABLE 1. Specification of IM.

Parameter	Values
Power rating	5HP/3.7kW
Voltage	415V
Winding Connection	Delta
Poles	4
Speed	1450 rpm
Frequency	50 Hz
Core length	194 mm
Stator outer diameter	165 mm
Stator inner diameter	85 mm
Air gap length	0.5 mm
Rotor inner diameter	35 mm
Number of stator slots	60
Number of rotor slots	51
Number of Turns	480
Number of Layers	2

In general, the motor with a larger diameter produces more torque with less speed, whereas the motor with a small diameter produces less torque with high speed. This is due to the increase in flux density resulting in the decreased motor size. Increased flux density above the rated specification reduces the motor diameter, magnetic core becomes saturated and this saturation will cause overheating and may result in the failure of the motor operation. To overcome this limitation, the length of the motor, operating temperature, size of the wires, torque, and speed must be adequately balanced. Importantly, the design of the motor relies on its length and diameter. Moreover, the length and diameter are determined by the application [37].

The materials used for manufacturing motor and the geometrical factors like core and winding dimensions are the most important factors in designing the motor. Moreover, proper selection of material can improve motor efficiency. The proposed IM design [38], is chosen for diagnosis the fault condition in efficient IM [39], [40]. Various motor parameters considered for the motor design is depicted in Fig. (1).

The geometrical specification and design of IM are explained in the following subsections.

A. STATOR GEOMETRY

The stator geometry is designed based on the core depth, slot depth, teeth width, slot width, and slot height. These parameter equations are given as follows,

1) STATOR CORE DEPTH (d_{cs})

The maximum flux density (${B_{cs}}^{max}$), occurs at the stator core depth(${d_{cs}}^{min}$) and it is given by,

$$ {d_{cs}}^{min} = 10^3 \frac{\phi}{4L_i} \tag{1} $$

where N_s is the number of conductors per phase and (ϕ) is the per phase magnetic flux given by,

$$ \phi = 10^3 \frac{E_{sph}}{4.44 f \phi K_d} \tag{2} $$

where f, K_d, E_{sph} are frequency, distribution factor, and induced EMF of stator phase respectively.

$$ N_s = \frac{E_{sph}}{4.44 f \phi K_d} \tag{3} $$

where,

$$ K_d = \int \left(10^3 \frac{sin(4\pi/9m)}{sin\left(\frac{4\pi p}{9S_s}\right) S_s} + 0.5 \right) 10^{-3} \tag{4} $$

where, p, S_s, m are the poles, Stator slots, and number of phases. Then, the motor's core length L_i is obtained as,

$$ \text{Core Length}(\mathrm{L_i}) = S_f L \tag{5} $$

where, L and S_f are active length and stacking factor.

2) STATOR SLOT DEPTH (d_{ss})

$$ {d_{ss}}^{max} = 10^3 \left(\frac{D_0 - D - 2{d_{cs}}^{min}}{2} \right) \tag{6} $$

where D, D_0, d_{cs} are denoted as inner diameter, outer diameter, and stator core depth respectively. Here, substituting (2) and (5) in (1),

$$ {d_{cs}}^{min} = 10^3 \left(\frac{10^3 \frac{E_{sph}}{4.44 f_e \phi K_d}}{4 S_f L} \right) \tag{7} $$

Substituting (7) in (6).

$$ {d_{ss}}^{max} = 10^3 \frac{D_0 - D - 2 * 10^3 \left(\frac{10^3 \frac{E_{sph}}{4.44 f_e \phi K_d}}{4 S_f L} \right)}{2} \tag{8} $$

3) STATOR TEETH WIDTH (W_{ts})

The maximum flux density (${B_{ts}}^{max}$), that occurs at the stator teeth that influence both the Width of the stator teeth (W_{ts}) and width of the stator slot (B_{ss}), is given as,

$$ {W_{ts}}^{min} = 10^3 \frac{p\phi}{2.2 S_r L_i} \tag{9} $$

where S_s and S_r are stator slots and rotor slots. Here, substituting (2) and (5) in (8).

$$ W_{ts} = \frac{\pi(D + d_{ss}) - S_s B_{ss}^{max}}{S_s} \tag{10} $$

where,

$$ {B_{ss}}^{max} = \frac{\pi(D + d_{ss}) - {W_{ts}}^{min}}{S_S} $$

4) STATOR SLOT WIDTH (B_{ss})

Stator slot width at teeth, at opening and at the end is denoted as $B_{ss1}, B_{ss2}, B_{ss3}$. They are expressed as,

$$B_{ss1} = \frac{\pi D - 10^3 \frac{p\phi}{B_{ts} L_i}}{S_s} \tag{11}$$

$$B_{ss2} = \frac{\pi(D + d_{ss}/5) - S_s W_{ts}}{S_s} \tag{12}$$

$$B_{ss3} = \frac{\pi(D + 2d_{ss}) - S_s W_{ts}}{S_s} \tag{13}$$

5) STATOR SLOT HEIGHT (h_s)

Stator slot height at teeth, at opening and at the end is denoted as h_{s0}, h_{s1}, h_{s2} and they are expressed as,

$$h_{s0} = d_{ss}/30; \;\; h_{s1} = d_{ss}/15; \;\; h_{s2} = d_{ss} - h_{s0} - h_{s1}$$

B. ROTOR GEOMETRY

Rotor geometry parameters like rotor diameter, core depth, teeth width and bar cross-sectional area are used for designing the motor and the following equation is utilized.

1) ROTOR DIAMETER (D_r)

The rotor diameter can be obtained as follows,

$$D_r = D - 2l_g \tag{14}$$

2) ROTOR CORE DEPTH (d_{cr})

The maximum flux density (B_{cr}^{max}), that occurs at the rotor core depth is given as,

$$d_{cr} = 10^3 \frac{\phi}{2B_{cr}{}^{max} L_i} \tag{15}$$

Substituting (13) and (14) in (15) rotor slot depth is given by,

$$d_{sr} = \frac{D_r - D_{shaft} - 2d_{cr}}{2} \tag{16}$$

3) ROTOR COPPER LOSS

The maximum shaft diameter can be specified in order to limit the saturation level of the rotor core. Rotor resistance (R_r) is designed to reduce rotor copper losses ($P_r{}^{cu}$) as follows,

$$P_r{}^{cu} = R_r I_{br}{}^2 \tag{17}$$

where,

$$R_r = \frac{r_{br}}{(N_s{}^{eff}/N_r{}^{eff})} + K_r r_{rr} \left(\frac{I_{rr}}{I_{br}}\right)^2 \tag{18}$$

In (18), $(N_s{}^{eff}/N_r{}^{eff})$ is the ratio of the effective stator and rotor turns. Here, the rotor bar and rotor ring resistances are expressed as r_{br}, r_{rr}, then rotor bar and rotor ring currents are denoted as I_{br} *and* I_{rr}, respectively given by the following equations,

$$\left(\frac{N_s{}^{eff}}{N_r{}^{eff}}\right) = \frac{\sqrt[2]{mK_w} N_s}{S_r}$$

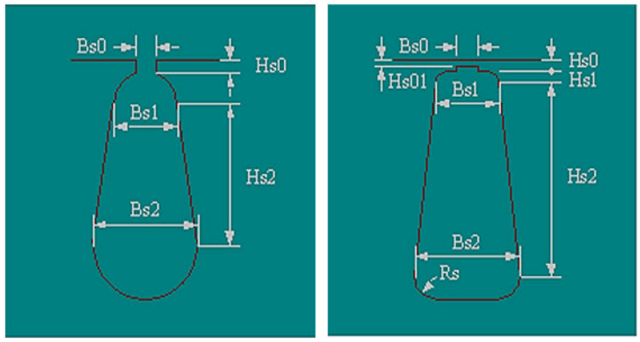

FIGURE 2. Slot Specification of Stator(left) and Rotor(right).

Here, Rotor bar resistance (r_{br}),

$$r_{br} = \frac{2.7 * 10^{-5} S_r{}^2 L \Psi \delta_s}{0.8 Z_s I_{sph}}$$

Rotor ring resistance (r_{rr}),

$$r_{rr} = \frac{2.7 * 10^{-3} \pi (D_r + 3D_{shaft})}{5(D_r - D_{shaft})}$$

Rotor bar current (I_{br}),

$$I_{br} = \frac{2mK_w N_s I_{sph} cos\varphi}{S_r}$$

and Rotor ring current (I_{rr}),

$$I_{rr} = I_{br} \frac{S_r}{\pi p}$$

where K_w, N_s, δ_s, I_{sph}, Z_s, and Ψ are denotes as winding factor, number of stator turns, Stator conductors current density, phase current, number of conductors, and number of Parallel circuits.

4) ROTOR TEETH WIDTH (W_{tr})

$$W_{tr} = \frac{\pi(D_r - d_{sr}) - S_r W_{sr}}{S_r} \tag{19}$$

where the rotor slot width is,

$$W_{sr} = \frac{\pi \left(\sqrt{\frac{4a_{br}}{\pi}} + 0.4\right)^2}{4d_{sr}}$$

5) ROTOR BAR CROSS-SECTIONAL AREA (a_{br})

$$a_{br} = 0.8 \frac{Z_s I_{sph}}{\Psi \delta_s S_r} \tag{20}$$

Fig. (2) represents IM stator and rotor Slot and the Geometry specifications designed using the above equations is given in Table. (2).

TABLE 2. Geometry specification of IM.

Parameter	Values
Stator and Rotor slot width at teeth (B_{s0})	0.33 and 0.33 inches
Stator and Rotor slot width at opening (B_{s1})	0.13 and 0.07 inches
Stator and Rotor slot width at end (B_{s2})	0.19 and 0.11 inches
Stator and Rotor slot height at teeth (H_{s0})	0.02 and 0.01 inches
Stator and Rotor slot height at end (H_{s2})	0.98 and 0.39 inches
Rotor slot height at opening (H_{s01} and H_{s1})	0.02 and 0.01 inches
Stator Teeth Flux Density	1.35 Wb/m^2
Rotor Teeth Flux Density	1.55 Wb/m^2
Air-Gap Flux Density	0.488 Wb/m^2
Specific Electric Loading	43.29 A/mm^2
Stator Winding Factor	0.83
Stacking Factor	0.95

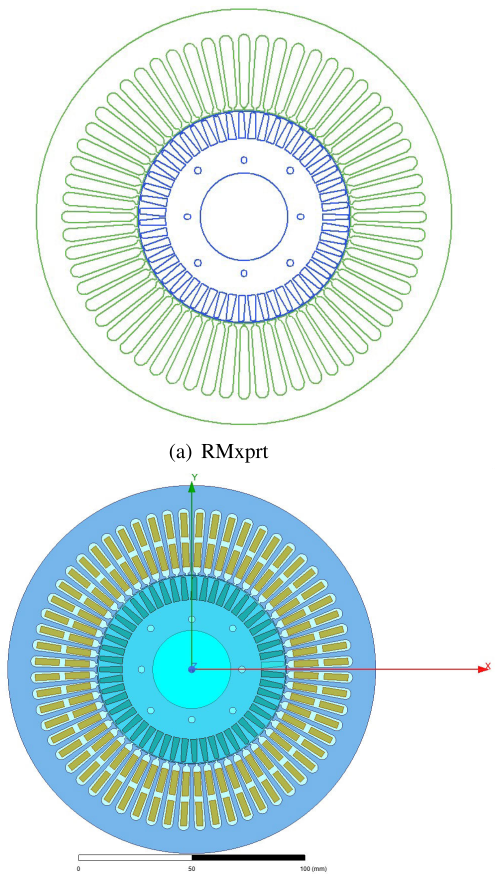

(a) RMxprt

(b) 2D MAXWELL

FIGURE 3. Geometrical models of induction motor.

III. DESIGN AND ANALYSIS OF IM USING FEA

Finite Element Analysis (FEA) is used to analyze the material for designing the 5HP motor with better efficiency for EV application. The selection of material relies on its mass and cost of it. The structure of IM is designed using ANSYS with optimized specifications like dimensions, core, and winding material [41]. Carbon steel 1008 as core and Cu as winding material provided better efficiency, torque, power factor, and slip performance in our previous study [38].

Hence, these materials are used for the design of IM in RMxprt and 2D Maxwell in ANSYS platform. The cross-sectional view of the motor designed is shown in Fig. (3), and the motor specifications are given in Table. (1).

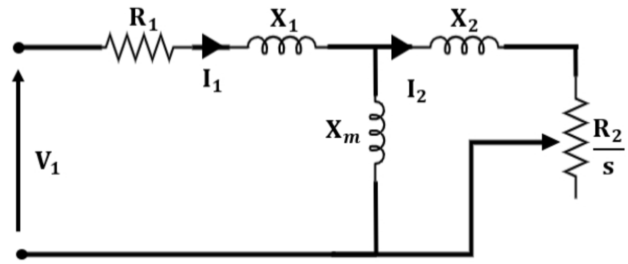

FIGURE 4. Equivalent circuit of an IM.

The per phase equivalent circuit of IM is given in Fig. (4). Here, R_1, R_2 are stator and rotor resistances respectively, X_1, X_2 are stator and rotor leakage reactance respectively, X_m is magnetizing reactance, and s is slip [42]. The electrical parameters of the proposed IM obtained from ANSYS design is $R_1 = 1.64\ \Omega$, $R_2 = 1.97\ \Omega$, $X_1 = 8.41\ \Omega$, $X_2 = 7.17\ \Omega$, $X_m = 114.19\ \Omega$, and s = 0.05.

The per phase impedance from Fig. (4) is

$$Z_{ph} = R_1 + jX_1 + \frac{Z_2 Z_m}{Z_2 + Z_m} \tag{21}$$

where $Z_2, Z_m,$ and R_2' are given by,

$$Z_2 = R_2' + jX_2,\ Z_m = jX_m,\ \text{and}\ R_2' = \frac{R_2}{s}$$

Equation (21) can be expressed as,

$$Z_{ph} = R_{ph} + jX_{ph} \tag{22}$$

where,

$$R_{ph} = R_1 + \frac{R_2' X_m^2}{{R_2'}^2 + (X_m + X_2)^2}$$

$$X_{ph} = X_1 + \frac{X_m {R_2'}^2 + X_m X_2 (X_m + X_2)}{{R_2'}^2 + (X_m + X_2)^2}$$

These per phase values are calculated from the designed IM's stator and rotor parameters as $R_{ph} = 33.19\ \Omega$ and $X_{ph} = 25.40\ \Omega$. For the proposed design the core loss is 0.002 W, and the stator and rotor copper losses are 238.7 W and 236.3 W, respectively.

The pitch factor is one of the important design parameter that enhances the performance of IM [43].

$$\text{Pitch factor } (\mathrm{K_p}) = \cos\frac{\alpha}{2} \tag{23}$$

where, α is the short pitch angle given by,

$$\alpha = \frac{180^\circ}{\text{coil span}}$$

where,

$$\text{Coilspan} = \frac{\text{Total Number of Stator slots}}{\text{Number of poles}}$$

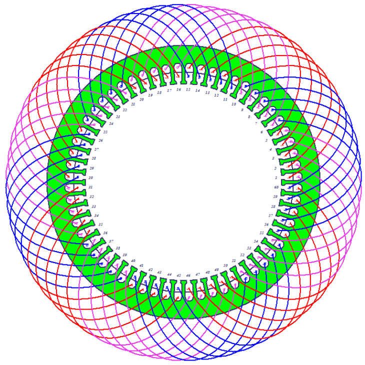

FIGURE 5. Stator winding pattern.

For a pitch short angle α of 12°, the pitch factor $(K_p) = 0.99$, distribution factor $(K_d) = 0.95$ and hence the winding factor (K_W) is 0.94. Double layer stator winding pattern is used in the proposed IM model and the winding pattern designed using ANSYS is shown in Fig. (5).

Based on the design consideration, Healthy and faulty conditions are created by integrating RMxprt with the Simplorer model in ANSYS, and the developed model is used for FDD. Load variation is given to the Healthy and Faulty motor model. The motor faults are created in the stator winding as a SC fault [44], HRC, and OPC fault as depicted in Fig. (6). The performance of the designed IM is analyzed with various loads. The RMS data of motor parameter such as stator currents (I1, I2, I3), and torque is extracted from the simulated motor designed, for healthy and faulty conditions at different load settings from Simplorer. A sample of data obtained for 80kg (0.0245 kgm^2) load is shown in Fig. (8). The healthy motor produced an efficiency of about 85% at a speed of 1437.122 rpm with torque 9.8 Nm. The faulty motor data is obtained for two different cases. In case I, fault is created at $t = 0$ and the fault is applied throughout the simulation. In case II, motor is run as a healthy motor from $t = 0s$ to $0.5s$ and further the fault is created at $t = 0.5s$. The Short circuit fault is created between the phase A & B, B & C, and C & A. Similarly, HRC and Open phase circuit are created at each phases A, B, and C of the motor supply terminal. Machine learning is used to predict the condition of the motor (healthy or faulty) from the collected data.

IV. FAULT DIAGNOSIS OF IM USING ML

FD strategy is implemented through data driven ML approach to predict the three phase supply connection failures in IM. The Data is obtained from the Simplorer platform. The healthy and various faulty conditions of IM are analysed in this study. Stator winding failure is one among the most common failure modes in IM. HRC faults can be caused due to human error during the motor assembly. Additionally, SC connection and OPC fault are also found as the reason for motor failure. Hence, industries are more interested in diagnosing these failures to overcome human errors [19], [45].

TABLE 3. List of labels.

Label	Values
1	Healthy ABC
2	Short Circuit AB
3	Short Circuit BC
4	Short Circuit CA
5	HRC A
6	HRC B
7	HRC C
8	Open Phase A
9	Open Phase B
10	Open Phase C
11	Short Circuit HF AB
12	Short Circuit HF BC
13	Short Circuit HF CA
14	Imbalanced data A
15	Imbalanced data B
16	Imbalanced data C

A. CLASSIFICATION OF DATA FOR THE HEALTHY AND FAULTY CONDITIONS OF IM AND LABEL GENERATION

Data sets obtained from the simulation platform are classified as healthy and faulty using ML classification algorithms and the list of labels used in this study is shown in Table. (3). From the total 4000 data, 250 data are classified as healthy and the remaining data are classified as faulty. Under faulty condition, data is further classified into 19 different classes and each class contains 250 sample data. As, HRC and OPC showed similar wave pattern for the motor parameters current, torque, slip, and efficiency in Case II (Healthy & Faulty) condition in simulation and they are grouped as same cluster, named as imbalanced fault. The total number of classes are 16 and their details are given in the Table. (3). The classified data is fed to ML to differentiate healthy and faulty condition of the motor.

B. DATA PROCESSING AND ML ALGORITHM

From the simulated model, 16 different healthy and faulty conditions are considered for data collection as given in Table. (3). The input features considered for data collection are, the phase currents, torque, slip, and efficiency. Label encoder is used to normalize the labeled data without any reduction in dimension, since there are minimal feature set. Finally, the normalized feature vectors are given as input to various ML algorithms.

The objective of all the ML algorithms is to distinguish between healthy and faulty classes, and the model is trained using a set of data with healthy and faulty classes that have been labeled already. This is done for all eight ML algorithms namely Support vector Machine (SVM), K-nearest neighbors (k-NN), Multi-layer perceptron (MLP), Random Forest (RF), Decision Tree (DT), Gradient boosting (GB), Extreme Gradient Boosting (XGBoost), and Deep Learning (DL) are used for classification of IM conditions. The data is split into 80:20 as training and test set. Grid search approach was used to select the ideal hyper parameters. Table. (4) provides the model settings and hyper parameters used for machine learning methods that can provide good precision

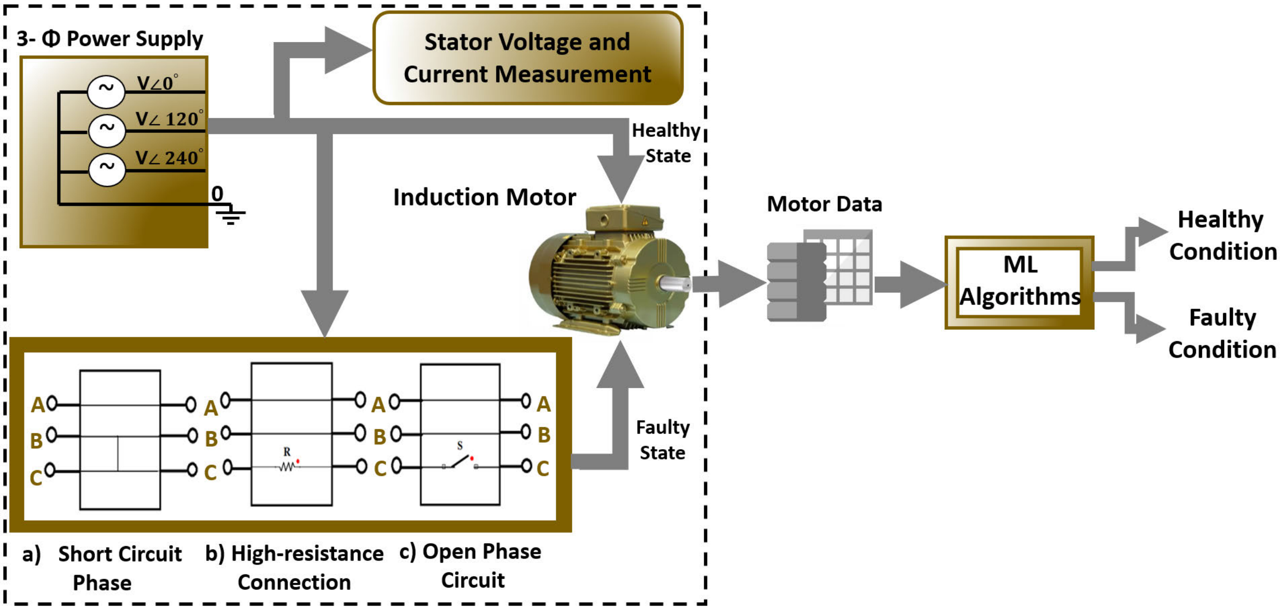

FIGURE 6. Schematic diagram of fault diagnosis in IM.

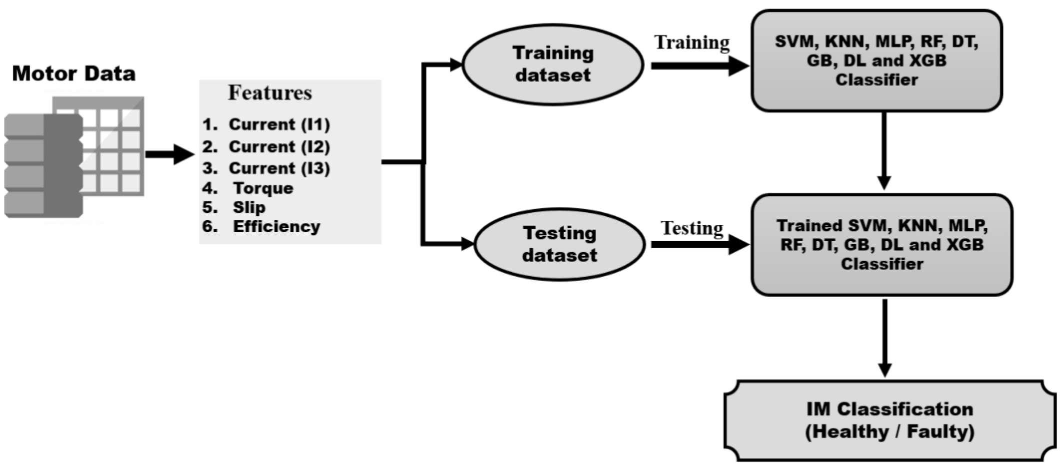

FIGURE 7. Schematic diagram of ML process.

TABLE 4. Machine learning parameters.

S.No	Models	Description
1	SVM	Regularization parameter (C)=1000, Kernel coefficient (gamma) =0.1
2	KNN	Number of neighbors : 3
3	MLP	Activation function = Rectified linear unit (relu), L2 regularization term (alpha)= 0.05, Number of neurons: 25, Maximum number of iterations: 100
4	RF	Number of trees (n_estimators): 300, Minimum number of samples (leaf node): 8, Bootstrap samples: False
5	DT	Minimum number of samples (split in internal node): 8, Leaf node: 2, Maximum depth: 5, Criterion: entropy
6	GB	Number of trees (n_estimators): 300, Learning rate (LR): 0.1
7	XGB	Minimum sum of instance weight needed in a child (min_child_weight): 5, Maximum depth: 3, Learning rate (LR): 0.25, Minimum loss reduction (gamma): 0.5, Subsampling ratio of columns for tree (colsample_bytree): 0.8
8	DL	Loss: sparse categorical crossentropy, Optimizer: adam, Metrics: accuracy

and accuracy for unknown data. Later, the trained model is further validate by test set. The test data used for the performance evaluation of each model. The performance of algorithms are evaluated by the confusion matrix as shown in

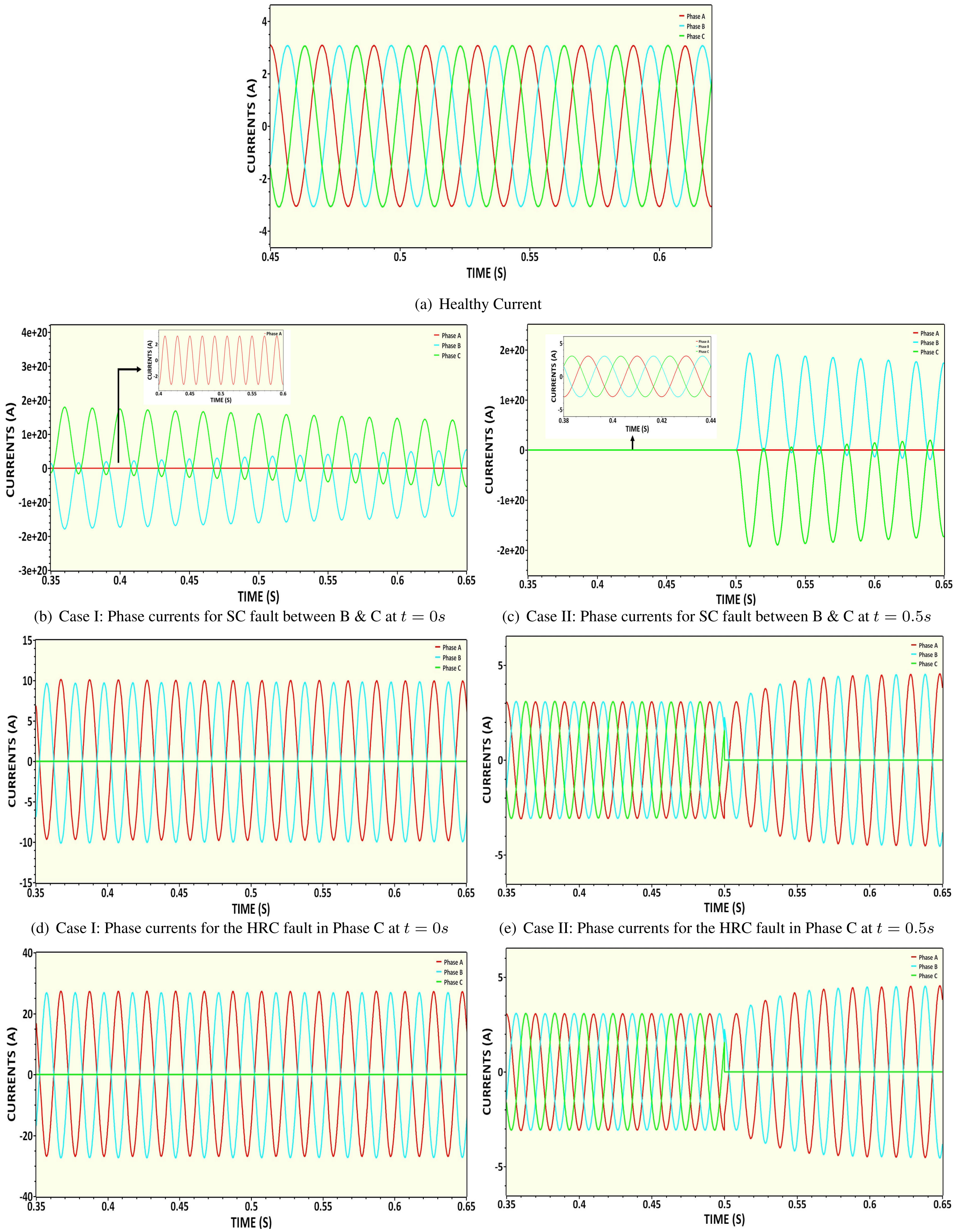

(a) Healthy Current

(b) Case I: Phase currents for SC fault between B & C at $t = 0s$

(c) Case II: Phase currents for SC fault between B & C at $t = 0.5s$

(d) Case I: Phase currents for the HRC fault in Phase C at $t = 0s$

(e) Case II: Phase currents for the HRC fault in Phase C at $t = 0.5s$

(f) Case I: Phase currents for the OPC fault in Phase C at $t = 0s$

(g) Case II: Phase currents for the OPC fault in Phase C at $t = 0.5s$

FIGURE 8. **Simulation results for the healthy and faulty conditions of IM using ANSYS.**

Fig. (9) which gives the comparison of predicted class label and the true class label. Also, its visual representation is given as Receiver operating characteristic (ROC) Curve as shown in Fig. (10). These evaluation metrics provide the performance

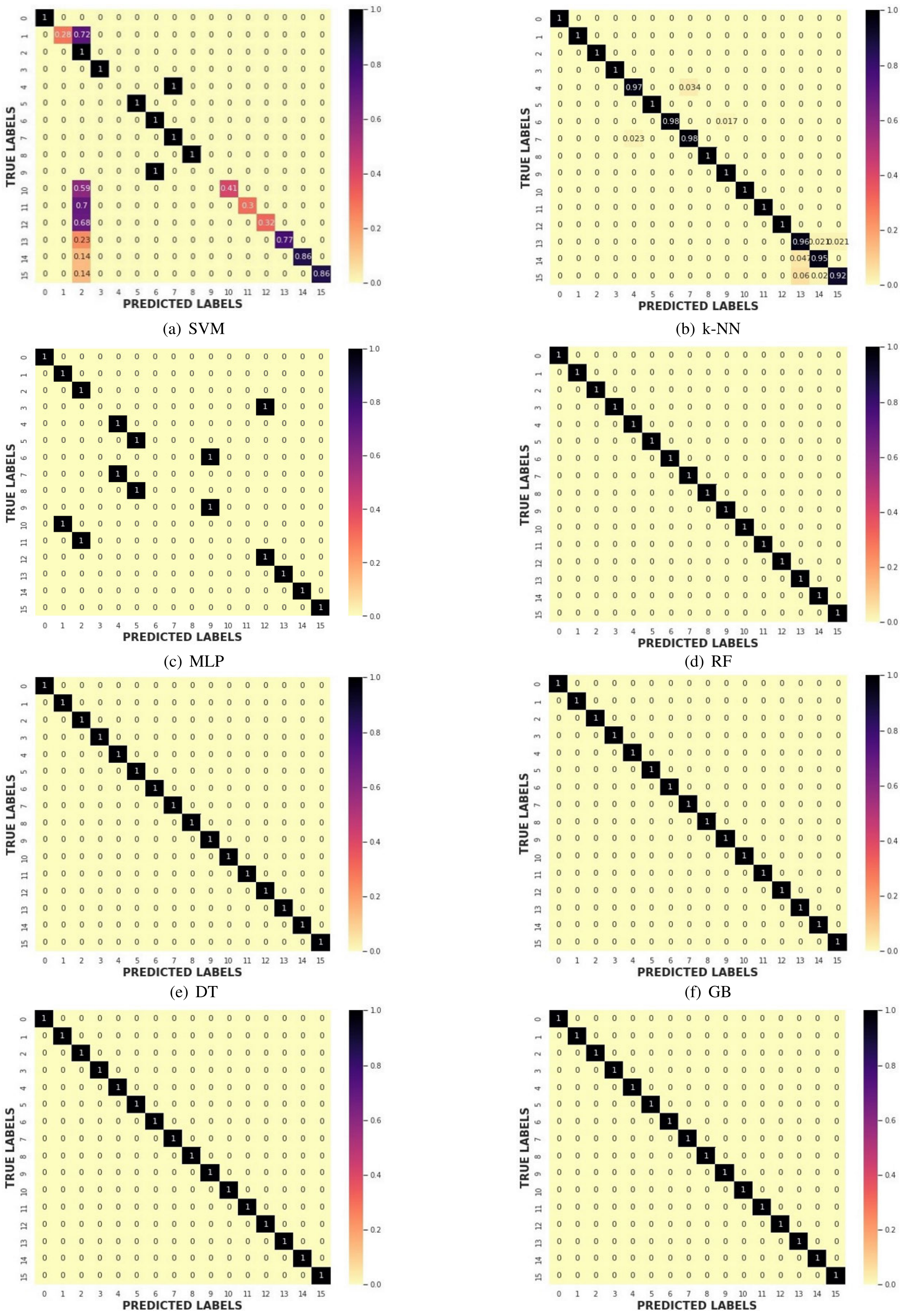

(a) SVM (b) k-NN (c) MLP (d) RF (e) DT (f) GB (g) XGB (h) DL

FIGURE 9. Confusion matrix algorithms for IM conditions.

of the model and it is used to compare with different ML algorithm.

The accuracy of different algorithms has been descried in the Table. (5). Due to the hyperparameter tuning, the SVM

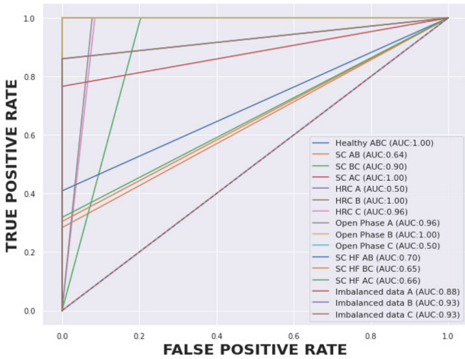

(a) SVM

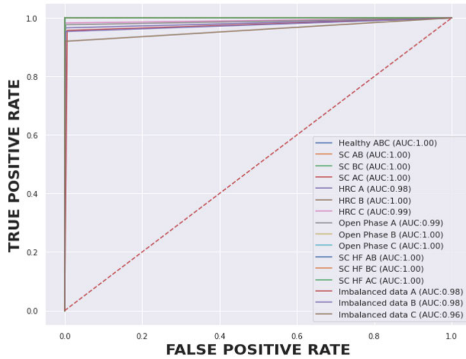

(b) kNN

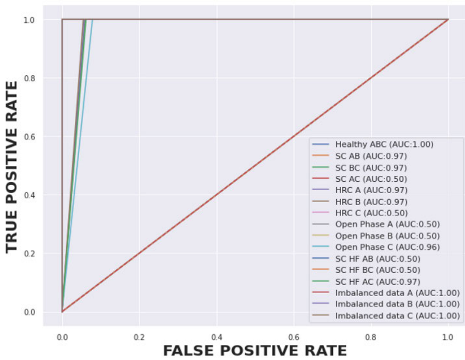

(c) MLP

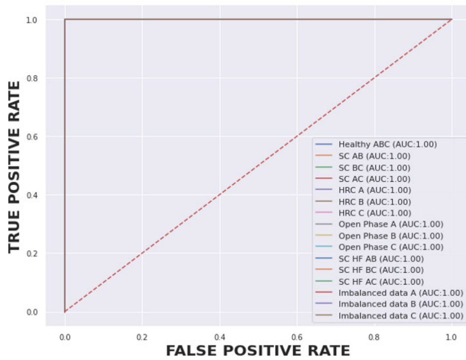

(d) RF

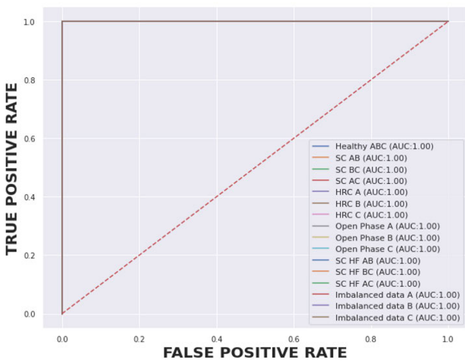

(e) DT

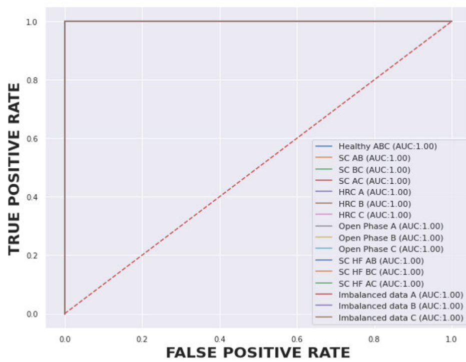

(f) GB

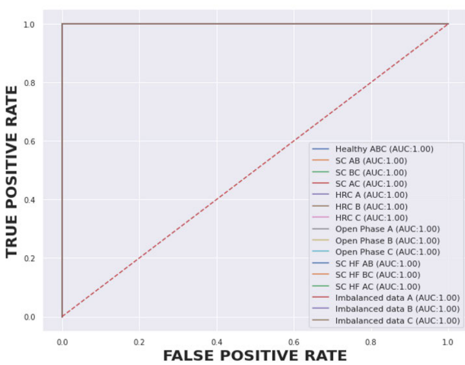

(g) XGB

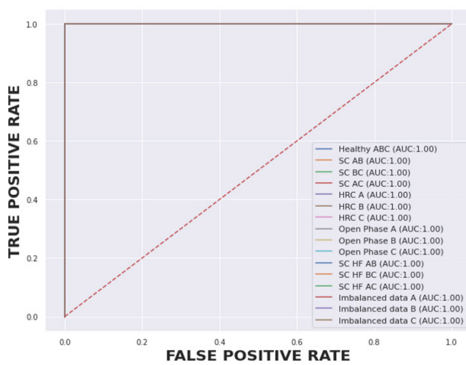

(h) DL

FIGURE 10. ROC for ML algorithms.

approach gives 65% accuracy. Fig. (9a), shows that, some of the test data/labels are misclassified to class 3 of predicted labels, and the true class labels of 5 and 10 are inappropriately assigned to the predicted class label of 8 and 7, respectively. The MLP algorithm provides 64% accuracy due to the misclassification of six classes of test data as dipicted in Fig. (9c).

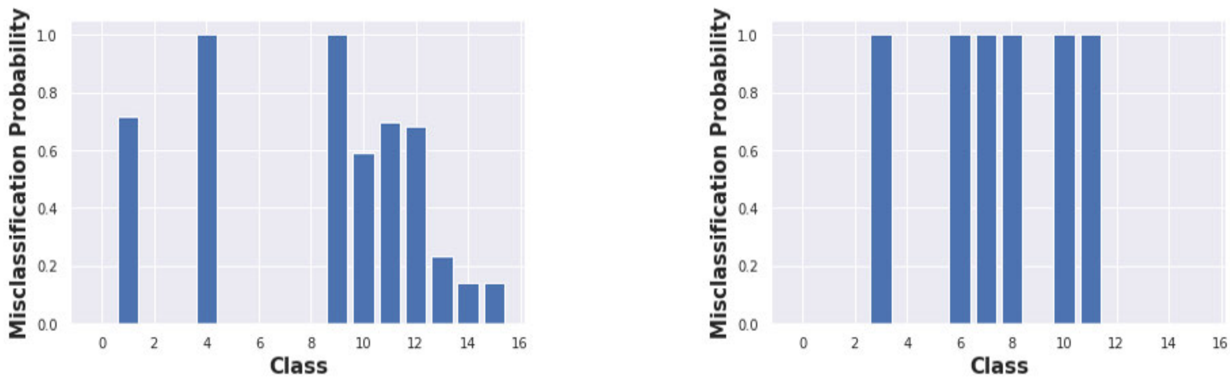

(a) Misclassification Probability of SVM Classifier (b) Misclassification Probability of MLP Classifier

FIGURE 11. Misclassification of ML algorithms.

TABLE 5. Accuracy & ROC of various ML models in diagnosis IM faults.

S.No	Algorithms	Accuracy (%)	ROC
1	SVM	65	0.82
2	KNN	98	0.99
3	MLP	65	0.80
4	RF	100	1
5	DT	100	1
6	GB	100	1
7	XGB	100	1
8	DL	100	1

In this, true labels of 6, 7, 8, 11, 12, and 13 are inappropriately assigned to the predicted labels of 9, 10, 5, 2, 3 and 4 respectively. The probability of misclassification is depicted in Fig. (11a, 11b), which shows that the misclassification varies from '0 to 1'; where '1' denotes 100% misclassification. Due to the minimal misclassification of test data, the k-NN is provide an accuracy of 98% as given in Fig. (9b). Apart from this, other algorithms such as RF, DT, GB, XGBoost, and DL produced the best value of accuracy (100%) in healthy and faulty conditions as given in Fig. (9d, 9e, 9f, 9g,9h). Therefore, these ML models are selected at the end of the training/testing process for the FDD of IM EV.

V. CONCLUSION

This article describes the ML-based FDD strategy for IMs under Healthy and Faulty condition. Data is generated using simulation-based models in ANSYS Simplorer for the proposed strategy. The data generated is used for training, validation, and testing various algorithms such as Support vector Machine (SVM), K-nearest neighbors (k-NN), Multilayer perceptron (MLP), Random Forest (RF), Decision Tree (DT), Gradient boosting (GB), Extreme Gradient Boosting (XGBoost), and Deep Learning (DL). To enhance the efficiency of the ML based FDD, feature extraction and selection methods are utilized for this model. By optimizing the K-nearest neighbors (k-NN), Random Forest (RF), Decision Tree (DT), Gradient Boosting (GB), Extreme Gradient Boosting (XGBoost), and Deep Learning (DL) algorithms provides superior results with an accuracy of 98% to 100%. Hence, these technique can diagnose the healthy and faulty conditions accurately. Also, the deployment of ML algorithms for FDD in EV application has the ability to extract important data features automatically which leads to flexibility and versatility. Moreover, the real time data analysis enables early fault identification, reduces downtime, lowers the maintenance cost, and provides better motor performance. In addition, the FD information can be used to design Fault Tolerant Control (FTC), that can provide better reliability and safety for the EV application.

REFERENCES

[1] P. B. Reddy, A. M. El-Refaie, S. Galioto, and J. P. Alexander, "Design of synchronous reluctance motor utilizing dual-phase material for traction applications," *IEEE Trans. Ind. Appl.*, vol. 53, no. 3, pp. 1948–1957, May/Jun. 2017.

[2] J. Zhu, K. W. E. Cheng, X. Xue, and Y. Zou, "Design of a new enhanced torque in-wheel switched reluctance motor with divided teeth for electric vehicles," *IEEE Trans. Magn.*, vol. 53, no. 11, pp. 1–4, Nov. 2017.

[3] C. C. Chan, A. Bouscayrol, and K. Chen, "Electric, hybrid, and fuel-cell vehicles: Architectures and modelling," *IEEE Trans. Veh. Technol.*, vol. 59, no. 2, pp. 589–598, Feb. 2010.

[4] J. Mei, Y. Zuo, C. H. T. Lee, and J. L. Kirtley, "Modeling and optimizing method for axial flux induction motor of electric vehicles," *IEEE Trans. Veh. Technol.*, vol. 69, no. 11, pp. 12822–12831, Nov. 2020.

[5] G. Singh, T. C. A. Kumar, and V. N. A. Naikan, "Induction motor inter turn fault detection using infrared thermographic analysis," *Infr. Phys. Technol.*, vol. 77, pp. 227–282, Jul. 2016.

[6] A. Boglietti, A. Cavagnino, M. Lazzari, and S. Vaschetto, "Preliminary induction motor electromagnetic sizing based on a geometrical approach," *IET Electr. Power Appl.*, vol. 6, no. 9, pp. 583–592, 2012.

[7] M. J. Akhtar and R. K. Behera, "Optimal design of stator and rotor slot of induction motor for electric vehicle applications," *IET Elect. Syst. Transp.*, vol. 9, no. 1, pp. 35–43, 2019.

[8] B. Tekgun, Y. Sozer, I. Tsukerman, P. Upadhyay, and S. Englebretson, "Core loss estimation in electric machines with flux-controlled core loss tester," *IEEE Trans. Ind. Appl.*, vol. 55, no. 2, pp. 1299–1308, Mar. 2019.

[9] S. Barg, K. Ammous, H. Mejbri, and A. Ammous, "An improved empirical formulation for magnetic core losses estimation under nonsinusoidal induction," *IEEE Trans. Power Electron.*, vol. 32, no. 3, pp. 2146–2154, Mar. 2017.

[10] J.-W. Kim, B.-T. Kim, and B. I. Kwon, "Optimal stator slot design of inverter-fed induction motor in consideration of harmonic losses," *IEEE Trans. Magn.*, vol. 41, no. 5, pp. 2012–2015, May 2005.

[11] D. Zhang, C. S. Park, and C. S. Koh, "A new optimal design method of rotor slot of three-phase squirrel cage induction motor for NEMA class D speed-torque characteristic using multi-objective optimization algorithm," *IEEE Trans. Magn.*, vol. 48, no. 2, pp. 879–882, Feb. 2012.

[12] L. Alberti, N. Bianchi, A. Boglietti, and A. Cavagnino, "Core axial lengthening as effective solution to improve the induction motor efficiency classes," *IEEE Trans. Ind. Appl.*, vol. 50, no. 1, pp. 218–225, Jan. 2014.

[13] H.-M. Yang, Z.-M. Pu, Z.-P. Guo, A. Zhang, and S.-M. Xiong, "A study of metal/die interfacial heat transfer behavior of vacuum die cast pure copper," *China Foundry*, vol. 17, no. 3, pp. 206–211, May 2020.

[14] I. Chasiotis, Y. Karnavas, and F. Scuiller, "Effect of rotor bars shape on the single-phase induction motors performance: An analysis toward their efficiency improvement," *Energies*, vol. 15, no. 3, p. 717, Jan. 2022.

[15] M. Z. Ali, M. N. S. K. Shabbir, X. Liang, Y. Zhang, and T. Hu, "Machine learning-based fault diagnosis for single- and multi-faults in induction motors using measured stator currents and vibration signals," *IEEE Trans. Ind. Appl.*, vol. 55, no. 3, pp. 2378–2391, May 2019.

[16] M. Sabouri, M. Ojaghi, J. Faiz, and A. J. M. Cardoso, "Model-based unified technique for identifying severities of stator inter-turn and rotor broken bar faults in SCIMs," *IET Electric Power Appl.*, vol. 14, no. 2, pp. 204–211, Feb. 2020.

[17] G. H. Bazan, A. Goedtel, O. Duque-Perez, and D. Morinigo-Sotelo, "Multi-fault diagnosis in three-phase induction motors using data optimization and machine learning techniques," *Electronics*, vol. 10, no. 12, p. 1462, Jun. 2021.

[18] G. H. Bazan, P. R. Scalassara, W. Endo, A. Goedtel, W. F. Godoy, and R. H. C. Palácios, "Stator fault analysis of three-phase induction motors using information measures and artificial neural networks," *Electr. Power Syst. Res.*, vol. 143, pp. 347–356, Feb. 2017.

[19] D. Gonzalez-Jimenez, J. Del-Olmo, J. Poza, F. Garramiola, and I. Sarasola, "Machine learning-based fault detection and diagnosis of faulty power connections of induction machines," *Energies*, vol. 14, no. 16, p. 4886, Aug. 2021.

[20] M. Z. Ali, M. N. S. K. Shabbir, S. M. K. Zaman, and X. Liang, "Single- and multi-fault diagnosis using machine learning for variable frequency drive-fed induction motors," *IEEE Trans. Ind. Appl.*, vol. 56, no. 3, pp. 2324–2337, May 2020.

[21] S. Shao, R. Yan, Y. Lu, P. Wang, and R. Gao, "DCNN-based multi-signal induction motor fault diagnosis," *IEEE Trans. Instrum. Meas.*, vol. 69, no. 6, pp. 2658–2669, Jun. 2020.

[22] F. B. Abid, M. Sallem, and A. Braham, "Robust interpretable deep learning for intelligent fault diagnosis of induction motors," *IEEE Trans. Instrum. Meas.*, vol. 69, no. 6, pp. 3506–3515, Jun. 2020.

[23] H. Kaplan, K. Tehrani, and M. Jamshidi, "A fault diagnosis design based on deep learning approach for electric vehicle applications," *Energies*, vol. 14, no. 20, p. 6599, Oct. 2021.

[24] Y. Xue, D. Dou, and J. Yang, "Multi-fault diagnosis of rotating machinery based on deep convolution neural network and support vector machine," *Measurement*, vol. 156, May 2020, Art. no. 107571.

[25] P. Kumar and A. S. Hati, "Deep convolutional neural network based on adaptive gradient optimizer for fault detection in SCIM," *ISA Trans.*, vol. 111, pp. 350–359, May 2021.

[26] J. J. Saucedo-Dorantes, M. Delgado-Prieto, R. A. Osornio-Rios, and R. D. J. Romero-Troncoso, "Multifault diagnosis method applied to an electric machine based on high-dimensional feature reduction," *IEEE Trans. Ind. Appl.*, vol. 53, no. 3, pp. 3086–3097, May/Jun. 2017.

[27] S. Langarica, C. Ruffelmacher, and F. Nunez, "An industrial internet application for real-time fault diagnosis in industrial motors," *IEEE Trans. Autom. Sci. Eng.*, vol. 17, no. 1, pp. 284–295, Jan. 2020.

[28] W. Zhang, C. Li, G. Peng, Y. Chen, and Z. Zhang, "A deep convolutional neural network with new training methods for bearing fault diagnosis under noisy environment and different working load," *Mech. Syst. Signal Process.*, vol. 100, pp. 439–453, Feb. 2018.

[29] P. M. D. La Barrera, G. R. Bossio, and J. A. Solsona, "High-resistance connection detection in induction motor drives using signal injection," *IEEE Trans. Ind. Electron.*, vol. 61, no. 7, pp. 3563–3573, Jul. 2014.

[30] J. Yun, K. Lee, K. W. Lee, S. B. Lee, and J. Y. Yoo, "Detection and classification of stator turn faults and high-resistance electrical connections for induction machines," *IEEE Trans. Ind. Appl.*, vol. 45, no. 2, pp. 666–675, Mar. 2009.

[31] M. Arkan, D. Kostic-Perovic, and P. J. Unsworth, "Modelling and simulation of induction motors with inter-turn faults for diagnostics," *Elect. Power Syst. Res.*, vol. 75, no. 1, pp. 57–66, 2005.

[32] M. Mengoni, L. Zarri, A. Tani, Y. Gritli, G. Serra, F. Filippetti, and D. Casadei, "Online detection of high-resistance connections in multiphase induction machines," *IEEE Trans. Power Electron.*, vol. 30, no. 8, pp. 4505–4513, Aug. 2015.

[33] D. Gonzalez-Jimenez, J. Del-Olmo, J. Poza, F. Garramiola, and P. Madina, "Data-driven fault diagnosis for electric drives: A review," *Sensors*, vol. 21, no. 12, p. 4024, Jun. 2021.

[34] J. F. Martins, V. F. Pires, and A. J. Pires, "Unsupervised neural-network-based algorithm for an on-line diagnosis of three-phase induction motor stator fault," *IEEE Trans. Ind. Electron.*, vol. 54, no. 1, pp. 259–264, Feb. 2007.

[35] R. A. Soman, N. M. Lokhande, and D. G. D. Bhardwaj, "Performance and analysis of 3 phase Induction motor using ANSYS Maxwell," *Int. J. Pure Appl. Math.*, vol. 118, no. 16, pp. 269–281, 2018.

[36] M. A. Iqbal and V. Agarwal, "Investigation & analysis of three phase induction motor using finite element method for power quality improvement," *Int. J. Electron. Electr. Eng.*, vol. 7, no. 9, pp. 901–908, 2014.

[37] Y. L. Karnavas and I. D. Chasiotis, "Influence of soft magnetic materials application to squirrel cage induction motor design and performance," *Eng. J.*, vol. 21, no. 1, pp. 193–206, Jan. 2017.

[38] M. Aishwarya and R. M. Brisilla, "Design of energy-efficient induction motor using ANSYS software," *Results Eng.*, vol. 16, Dec. 2022, Art. no. 100616.

[39] E. S. Hamdi, "Induction motor design," in *Design of Small Electrical Machines*. New York, NY, USA: Wiley, 1994, p. 260.

[40] J. Pyrhönen, "Properties of rotating electrical machines," in *Design of Rotating Electrical Machines*, 2nd ed. London, U.K.: Wiley, 2013, pp. 331–494.

[41] E. C. Abunike, O. I. Okoro, and G. D. Umoh, "Steady and dynamic states analysis of induction motor: FEA approach," *Nigerian J. Technol.*, vol. 36, no. 4, pp. 1202–1207, 2017.

[42] A. Gastli, "Identification of induction motor equivalent circuit parameters using the single-phase test," *IEEE Trans. Energy Convers.*, vol. 14, no. 1, pp. 51–56, Mar. 1999.

[43] J. S. Chapman, "Induction motors," in *Electrical Machinery Fundamentals*, 5th ed. New York, NY, USA: McGraw-Hill, 2012, pp. 307–396.

[44] P. Kumar and T. B. Isha, "FEM based electromagnetic signature analysis of winding inter-turn short-circuit fault in inverter fed induction motor," *CES Trans. Electr. Mach. Syst.*, vol. 3, no. 3, pp. 309–315, Sep. 2019.

[45] J. J. Lee, J. Singh, M. Azamfar, and V. Pandhare, "Industrial AI and predictive analytics for smart manufacturing systems," in *Smart Manufacturing*, M. Soroush, M. Baldea, and T. F. Edgar, Eds. Amsterdam, The Netherlands: Elsevier, 2020, pp. 213–244.

M. AISHWARYA received the bachelor's degree in electrical engineering from Anna University, in 2017, and the master's degree in power electronics and drives from the Vellore Institute of Technology (VIT), Vellore, India, in 2019, where she is currently pursuing the Ph.D. degree with the School of Electrical Engineering.

Her research interests include the design of electrical machines (ANSYS), transformer, fault diagnosis, and machine learning.

R. M. BRISILLA received the B.E. degree in electrical and electronics engineering from Manonmaniam Sundaranar University, India, in 2002, the M.E. degree in power electronics and drives from Anna University, India, in 2004, and the Ph.D. degree from the National Institute of Technology, Tiruchirappalli, in 2016.

She is currently an Associate Professor with the School of Electrical Engineering, Vellore Institute of Technology, Vellore, India. Her research interests include nonlinear systems and control, the control of drives and robotic systems, and fault diagnosis and control.